Si Vertex Upgrade: Status Report

H. Enyo, Y. Goto, N. Grau,
J. Haggerty, J. Heuser, J. Hill, D. Lee,
P. McGaughey, C.A. Ogilvie, H. Ohnishi, J. Rak,
K. Tanida, H. Van Hecke, S. White, C. Woody

May 21, 2002

Abstract

1 Introduction

This technical note outlines the status of work planning for a highly segmented, precise Si vertex detector in the inner region of PHENIX. We outline the physics case, specify the requirements, list possible technical options, and define the needed R&D. This note documents the state of work as of March 2002 and should be regarded as a work-in-progress. Many details are still being worked on, all geared towards the PHENIX Letter of Intent and R&D proposals.

2 Physics Overview

There are three broad areas of new physics that are made possible by the proposed Si vertex detector in PHENIX.

- a large increase in the range of x over which we can extract the gluon spin structure function in protons with measurements of open charm and beauty in polarized p+p reactions
- robust measurements of the shadowing of the gluon structure function in nuclei with measurements of open charm and beauty in p+A reactions

- probing the early, highest energy-density phase of the matter formed in a heavy-ion reaction by

  measuring the high-pt spectra of open charm. The energy-loss of high-pt heavy-quarks is predicted to be predominantly via medium-induced gluon radiation with negligible contribution from collision energy-loss, thus simplifying the connection between energy-loss and the properties of the medium.

  measuring the yields of both open-charm and beauty to firmly establish whether heavy-quarks are enhanced in the pre-equilibrium phase

  using the open charm yield to form the ratio (J/ψ)/(open charm) and hence to quantify the suppression of J/ψ

More details on each of these three goals can be found in the following sections.

2.1 Spin

The measured quark spin-structure function integrates to less than the required spin-1/2, a result that is described as the "spin-crisis"[1]. One leading possibility is that gluons carry the missing spin in the proton and as such PHENIX has a major goal of measuring the gluon spin-structure function in protons. PHENIX has existing capability for x$>$0.05 using direct-photons approximately back-to-back with a high-pt hadron. However this limited x-range is not broad enough to address the spin-crisis. The proposed Si vertex detector will enable the measurement of the spin asymmetry of open-charm and open beauty production covering the broad range $0.002 < x < 0.4$ (figure 1).

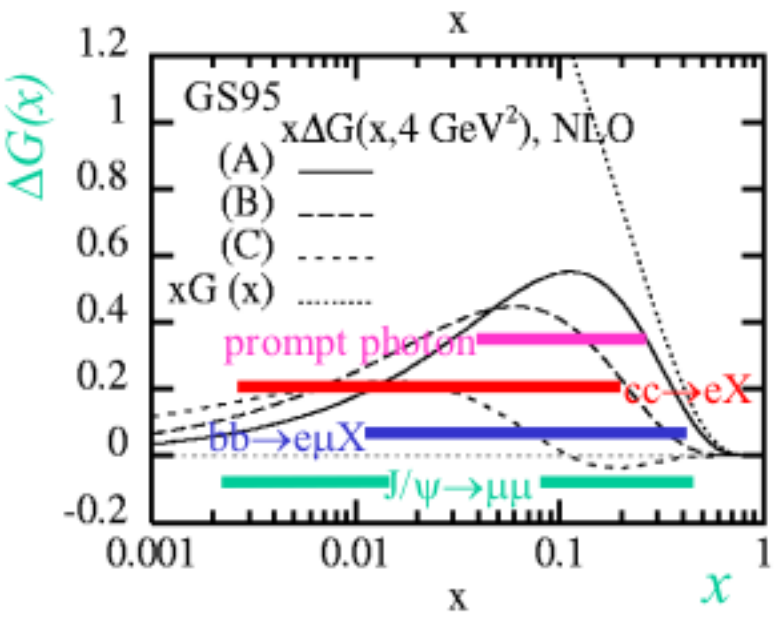

Figure 1: The gluon spin structure function as a function of x at Q^2=4 GeV^2 from Gehrmann-Sterling for different models and the experimental coverage for different channels in PHENIX.

This x-range is similar to that reached by measuring the spin asymmetry of J/ψ spectra in both the central arm and muon arms. However the link between J/ψ production and gluon structure function is fraught with model dependencies. It is difficult to calculate the soft-QCD evolution of the $c\overline{c}$ pair to the observed color singlet J/ψ[2]. It is therefore important to have other observables that are sensitive to the gluon spin-structure function but are not perturbed by the uncertainty of soft-QCD. The spin-asymmetry of open charm and beauty production both meet this requirement and therefore significantly extend PHENIX's capability to extract the x-dependence of the gluon spin structure function.

2.2 pp Heavy Flavor Production

Before using open charm and beauty for spin asymmetry measurements we need to test the next-to-leading-order (NLO) pQCD calculations for heavy-quark production[3, 4] by measuring the yield and pt spectra of open charm and beauty in proton+proton collisions. Previous comparisons have emphasized the total heavy-quark yield[3], but more stringent tests are possible with the pt spectra[5]. Qualitatively, low-pt charm and beauty production are dominated by gluon-fusion, while production at high-pt is expected to be dominated by the hard-scattered gluon splitting into a $Q\overline{Q}$ pair[6].

2.3 Gluon Structure Functions in Nuclei

The extraction of parton structure functions inside nuclei environment provides unique information on how partonic degrees-of-freedom are affected by a many-body system. A rich array of data has been collected[7] on how the quark-structure function is modified but little information exists on how the gluon-structure function is modified in nuclei[8, 9].

A key goal of the vertex upgrade is to provide robust measures of the gluon structure functions in nuclei over a broad range in x, $0.002 < x < 0.4$, by charm and beauty production. As can be seen in figure 2 this is the critical region where the structure function transitions from a region of suppression or shadowing (low-x) to anti-shadowing.

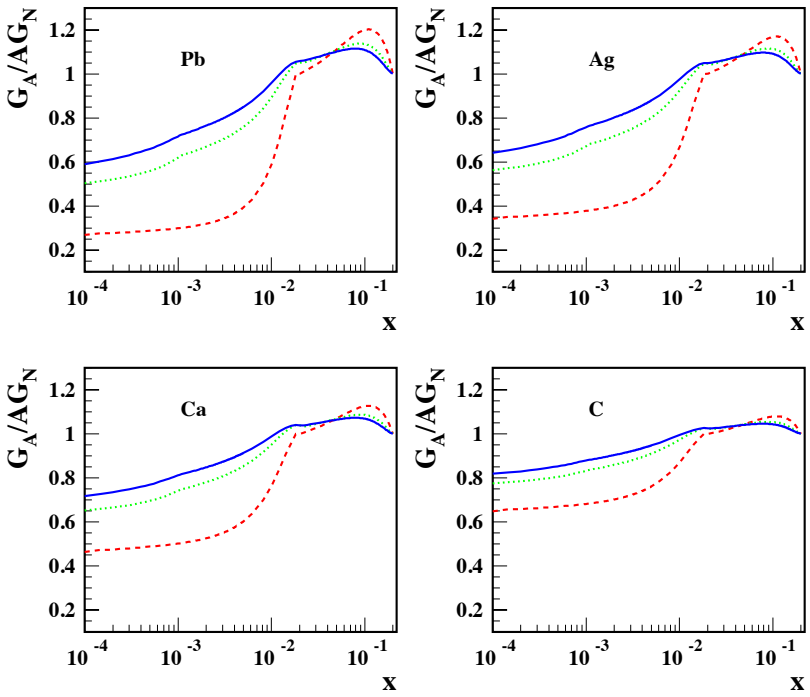

Figure 2: The relative gluon structure functions for different nuclei as a function of x for different nuclei[9]. The predictions for different momentum transfers of Q=2, 5, and 10 GeV are shown with dashed, dotted and solid curves respectively.

In particular the rapidity dependence of heavy-meson production shows sensitivity to the gluon suppression at low-x[5]. It is worth noting that J/ψ production cannot be used to extract gluon structure functions since the yield of J/ψ changes in a nuclear environment due to final state scattering of the $c\overline{c}$ pair as J/ψ is forming.[2].

A key question will be how to measure the relative luminosity in successive

pA runs to better than a few % in order to accurately measure the relative structure function in e.g. pAu to pp.

2.4 Probes of Early, Highest Energy-Density Stage of Heavy-ion Reactions

At the time of writing this technical note, it is not yet possible to state whether the quark-gluon plasma has been produced in nucleus-nucleus collisions at RHIC. In planning for upgrades to PHENIX, we have focused on the physics of the earliest, highest energy-density stage of these collisions. This stage will be important if either more evidence is required to answer whether the plasma has been formed, or instead the focus of RHIC physics has shifted from discovery to studying the properties of the plasma. In either scenario, the yield and spectra of heavy-flavor mesons will provide unique information on the earliest stages of a collision at RHIC, as is discussed in the following sub-sections.

2.4.1 Energy-loss of heavy-quarks

Colored high-pt partons are predicted to lose energy as they propagate through the medium[15]. The dominant mechanism is calculated to be medium-induced gluon radiation [16, 17] with a smaller contribution from elastic collisions with lower-energy partons[15]. Because of their larger mass, charm and beauty high-pt partons should have even less collision energy-loss[18] which would make the radiation energy-loss the dominant term[19, 20, 21, 22]. By having only one mechanism present, the energy-loss of heavy-quarks will provide a more robust connection to the properties of the medium. One open theoretical issue is whether the possibility of using non-relativistic-QCD for the the heavy-quarks make the theoretical calculations of energy-loss more reliable.

To exploit the physics of energy-loss will require measuring the pt spectra for open charm out to several GeV/c. Key will be measuring open charm spectra directly via the hadronic decay channels, e.g. $D \rightarrow K + \pi$. Depending on the signal to background in the reconstructed D invariant mass, we might also be able to correlate the reconstructed D with the pt and azimuthal distributions of other hadrons. Near-angle and back-to-back correlations open up alternative diagnostics of energy-loss in a dense medium.

PHENIX has extracted the cross-section for open charm in the momentum range pt$<$ 2 GeV/c via inclusive electron spectra[23]. However this result required

a large subtraction of background electrons from other sources, and at moderate to high-pt the spectrum receives contributions from both open charm and beauty.

With the Si vertex upgrade we can convert this first result into a robust measurement of the spectra of open charm out to high-pt. By selecting leptons that are displaced from the collision point we can reduce the contribution of background electrons and reduce the systematic error associated with their subtraction. We plan to subtract the beauty contribution at higher pt by using the distribution of lepton decay distances which will have a longer tail from the beauty contribution.

It is worthwhile emphasizing that the upgrade will provide PHENIX with two methods of extracting the charm spectra. Directly via hadronic decay, and deconvoluting the decay kinematics from the measured lepton spectra. These two will have different systematics and therir comparison will be important.

2.4.2 Open Charm and Beauty Enhancement

Open charm enhancement has been predicted in the earliest stages of A+A reactions[11, 12, 13]. Heavy-quarks are produced in the initial parton-parton collisions that occur during a heavy-ion reaction and possibly also via gluon fusion in the pre-equilibrium stage of the reaction. This is the mechanism originally proposed for strangeness enhancement, but may be more powerful in the case of charm because the rate of heavy-quark production is expected to be negligible later in the reaction when the energy density has decreased.

To firmly establish whether there is any enhanced pre-equilibrium charm production will require measuring open charm spectra over a wide range of pt from pp, pA and AA reactions. Measuring the yield of the heavier open-beauty in the same reactions will be a critical consistency check since open beauty should be less affected by pre-equilibrium production than open charm.

2.4.3 J/ψ Suppression

The suppression of J/ψ has been a long sought after signature of the plasma[14]. J/ψ that would form from $c\overline{c}$ pairs are either screened by the plasma or are broken up by interactions with semi-hard gluons. To quantitatively understand suppression requires knowledge of the initial production of $c\overline{c}$ pairs. The effectiveness of a deconfined medium in preventing the formation of J$/\psi$ can be quantified using the ratio J$/\psi$/(open charm).

2.5 Other Physics Topics

The Si vertex upgrade will help other physics programs in PHENIX. Simulations of these topics have not yet been done to quantify the level of improvement.

- narrow the mass-resolution for di-muon and di-electron invariant mass, opening up the possibility of upsilon spectroscopy
- improve high-pt tracking in the central arm by providing confirming hits close to the collision point. This will reduce the background tracks.
- increase the signal to background for all muon-pair combinations in the muon arms by removing muons from long-lived pion and kaon decay.
- measure multi-strange baryons, confirming STAR results that are likely to exist by the time of the upgrade.

2.6 Benefits of Forward and Mid-rapidity Coverage

Throughout this section we have emphasized the benefits of a broad coverage in rapidity for open charm and beauty. This will be possible with a Si vertex upgrade that consists of barrel and endcaps that match the PHENIX central and muon arms respectively. For convenience the advantages of a broad rapidity are collected here.

- a broad x-range to measure the spin gluon-structure function
- a broad x-range to measure the nuclear gluon structure function
- measuring the charm cross section in the same rapidity range as the J/ψ
- Energy loss of heavy quarks might be inferred from changes in the rapidity distribution.
- Charm cross section from the endcap and barrel will have different systematics. Even after cuts on the displaced vertex there will be residual background from conversion electrons and muons from hadron decays.
- The large acceptance muon arms will give much better statistics for all the charm and open beauty measurements discussed here.

3 Requirements and Strawman Detector

The performance requirements for the detector are

- ability to match tracks from central arm and muon arm to hits in multiple layers of the Si detector.
- sufficient position accuracy so that the displacement resolution of the track with respect to the collision point is less than the $c\tau$ of charm and beauty decays, i.e. a resolution less than 100μm, preferably at the level of 30-50 μm.
- for tracks at mid-rapidity the resolution needs to be predominantly in the rϕ direction, for tracks at forward/backward rapidity good resolution in both rϕ and z are required
- the detector must match the acceptance of the muon arms, the central arms, and the proposed HBD/TPC in the central arm

A variety of simulations and first principle calculations have shown that the displacement resolution is determined by the position accuracy of the two inner Si layers and by the amount of multiple-scattering between the collision point and the position measurements. A schematic estimate of how well the measurement of two positions can be extrapolated back to the collision point is

$$\sigma^2_{DCA} \sim \frac{(\Delta x_1)^2 + (\Delta x_2)^2}{separation^2} r^2 + \theta^2_{ms} r^2 + (\Delta x_1)^2 \qquad (1)$$

where Δx_1 and Δx_2 are the two position measurements from the inner two Si layers, r is the distance from the collision point to the first layer, $separation$ is the separation between the first two layers, and θ_{ms} is the multiple-scattering angle due to material in the beam-pipe and first-layer of Si.

To minimize the resolution, the first layer should be as close to the collision point as is practical, and the first layer plus beam-pipe should be as thin as possible. It should be noted that over a broad range of momentum multiple-scattering dominates and that the accuracy of the hit measurement is not the determining factor.

After exploring different configurations the working group decided on a semi-realistic strawman layout with reasonable thickness and positions for its Si layers. The strategy was to establish whether a reasonable strawman detector would be

able to meet our physics goals. We plan to iterate on the design, bringing in necessary details of the mechanics, layout, cooling, cabling etc..

The key dimensions of the strawman detector are tabulated in Table 1. The detector has four concentric barrels of silicon, which occupy the central 30 cm along the beam axis. The outer three barrel layers are Si strip detectors placed nominally at r=10cm (barrel 4) r=8cm (barrel 3) and r=6 cm (barrel 2). The inner barrel of silicon at r=2.5 cm is composed of pixel detectors (barrel 1). The beam-pipe is at r=2.0cm and is 500μm Be. The endcaps comprise of four disks of pixel detectors located at z= 16, 23 , 30 and 37 cm. Currently the radius of each disk increases from r= 12, 17, 22 and 26cm for the four disks. The inner radius for each disk is at 3.5cm

As a first step we set the thickness of each barrel and endcap layer to be 1% radiation length. This is meant to include detector, readout and cooling in a simplified one-volume effective layer. The value of 1% was chosen from a survey of built detectors.

In the strawman simulations, the pixel detectors for the inner barrel layer were assumed to have a segmentation of 50μm by 425μm, for the endcaps 50μm by 200μm. The endcap granularity is provisional and will most probably be changed due to the very large number of pixel channels for this granularity. The strip detectors (outer 3 layers) have a 80μm pitch and a strip length that is 3cm long. As described more fully in Section 6.4, each strip is read-out twice and with the second diagonal strip providing localization to 80μm by 800μm. This is not much larger than a Si pixel but requires a low occupancy environment to make the projective geometry work.

In order to maintain the occupancy below 10% in central Au-Au collisions, the area of the sensitive elements in barrel layer 2 should be smaller than $2.9 mm^2$. This is met by the candidate strip detectors that have a 80μm pitch, 3cm length for a surface area of $2.4 mm^2$. The occupancy is lower in the outer two barrel layers. One option to reduce the occupancy in barrel layer 2 would be to replace the Si strips with Si pixels.

4 Staging

Because the outer layers use Si strip-detectors, it will be possible to design and build the outer layers before the pixel technology is ready. There are two scenarios that the group is discussing

Table 1: Strawman Layout

part	detector	position	area (cm^2)	number channels
barrel 1	pixels	r=2.5cm, $\|z\| < 15cm$	470	2.2M
barrel 2	strips	r=6.0cm, $\|z\| <$ 15cm	1130	75K
barrel 3	strips	r=8.0cm, $\|z\| <$ 15cm	1510	100K
barrel 4	strips	r=10.0cm, $\|z\| <$ 15cm	1885	125K
endcap 1	pixels	$3.5 < r <$ 12cm, z=16cm	415	4.1M
endcap 2	pixels	$3.5 < r <$ 17cm, z=23cm	870	8.7M
endcap 3	pixels	$3.5 < r <$ 22cm, z=30cm	1480	14.8M
endcap 4	pixels	$3.5 < r <$ 26cm, z=37cm	2085	20.8M

- design and build the complete infrastructure (support, cooling, control, output etc.) for both the endcaps, inner layer of pixels, and outer three layers of strips. Implement the detector in stages, starting with the barrel layers using Si strips. The advantage of this strategy is that it requires only one mechanical design and integration with PHENIX, the disadvantage is that you have to specify at an early stage the cooling and infrastructure needed by the pixel layers.

- design and build a temporary mechanical support for the Si strips, replace that with a new support when the pixels are ready. The Si strip detectors and electronics are then placed back on the outer barrel layers of the new support. The disadvantage is that the large effort and cost of mechanical design/construction/interface with PHENIX is repeated.

5 Performance, simulations, rates

In the following sections, we describe the simulated performance of the strawman silicon vertex detector consisting of a central barrel region matched to the PHENIX central arms and two endcaps matched to the PHENIX muon arms. The simulations have been run within PHENIX's implementation of GEANT, PISA.

For convenience, we have separated each of the next sections into measurements possible with the central PHENIX arms plus the silicon barrel and those possible with the silicon endcaps and PHENIX muon arms. However, there are

some measurements listed below that require all of PHENIX's capabilities used in unison. The results shown below are work-in-progress and many details need to be worked on before PHENIX LOI and funding proposals can be written.

5.1 Open Heavy flavor

5.1.1 Open Charm Measurements

Central Arms - $D \rightarrow e + X$**,** $D \rightarrow K + \pi$

The four layers of the central silicon barrel provide an accurate measurement of the trajectory and impact parameter of tracks near mid-rapidity. Used together with the particle identification and momentum determined by the PHENIX central arms, charm decays can be identified. Electrons with a particular range of impact parameter and transverse momenta are primarily from semi-leptonic charm decays (once photon conversions have been removed from the data.) Exclusive charm decays, such as the $K + \pi$ channel can be fully reconstructed. These have the advantage of producing a peak at the D^0 mass, giving an unambiguous charm signal and direct extraction of the charm-meson spectrum.

Single electrons at different momenta were simulated through the strawman vertex detector. This simulation was run at zero-field and the hits from the electrons tracked back to calculate the transverse distance-of-closest approach to the known point-of-origin (figure 3).

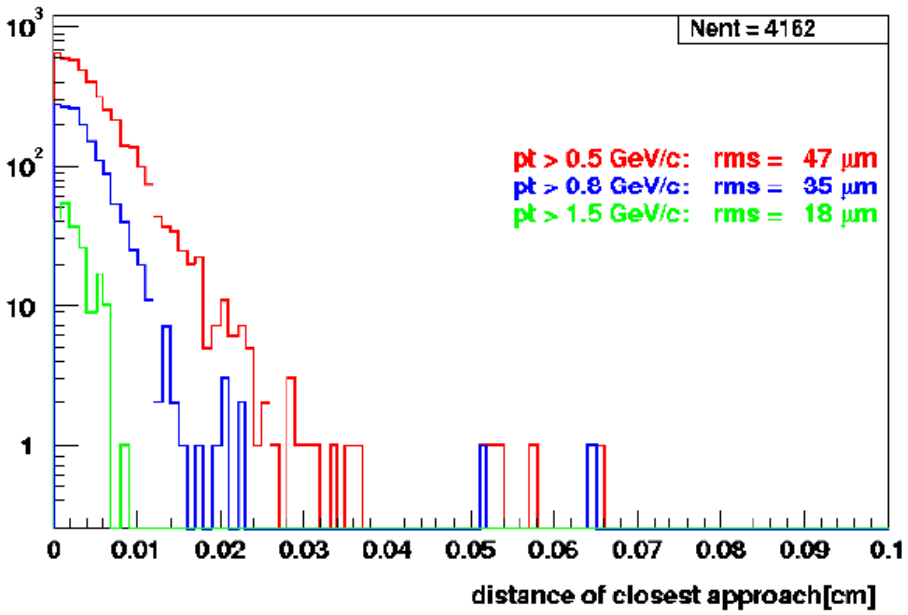

Figure 3: The transverse distance-of-closest approach to the known point-of-origin for electrons at different momenta as simulated through the strawman detector.

The rms value of these DCA distributions for electrons is less than 50μm, well below what is required to separate electrons from charm decay from other sources.

We generated a semi-realistic cocktail of hadronic decays, Dalitz decays, conversions, etc. (blue line in figure 4) together with electrons from charm decay (red line).

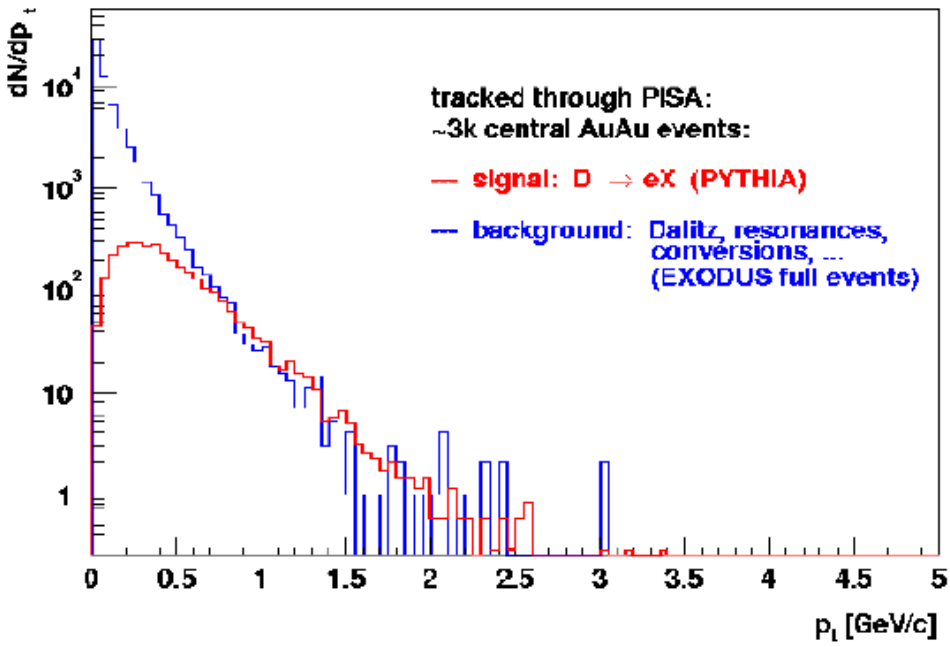

Figure 4: The momentum distribution of electrons from a semi-realistic cocktail of hadronic decays, Dalitz decays, conversions, etc. (blue line) together with electrons from charm decay (red line).

The relative scale of these two sources should be considered arbitrary. PHENIX's recent paper[23] uses the measured hadron spectra to constrain the cocktail which has not yet been done in our simulation. The goal of the current exercise is to quantify the effectiveness of a displacement cut on the tracks in removing the background and increasing the relative level of the charm signal/background (S/B). The next round of simulations will use constrained background sources.

Figure 5 shows the increase in the charm signal/background as larger DCA cuts are made. For DCA cuts larger than 100 μm the S/B reaches 4 for a momentum of 1 GeV/c. Applying such a DCA cut should produce an electron spectrum that is dominated by charm decays and, at high-momentum, beauty decays. One simulation that remains to be done is how accurately we can subtract the beauty contribution from the distribution of decay distances.

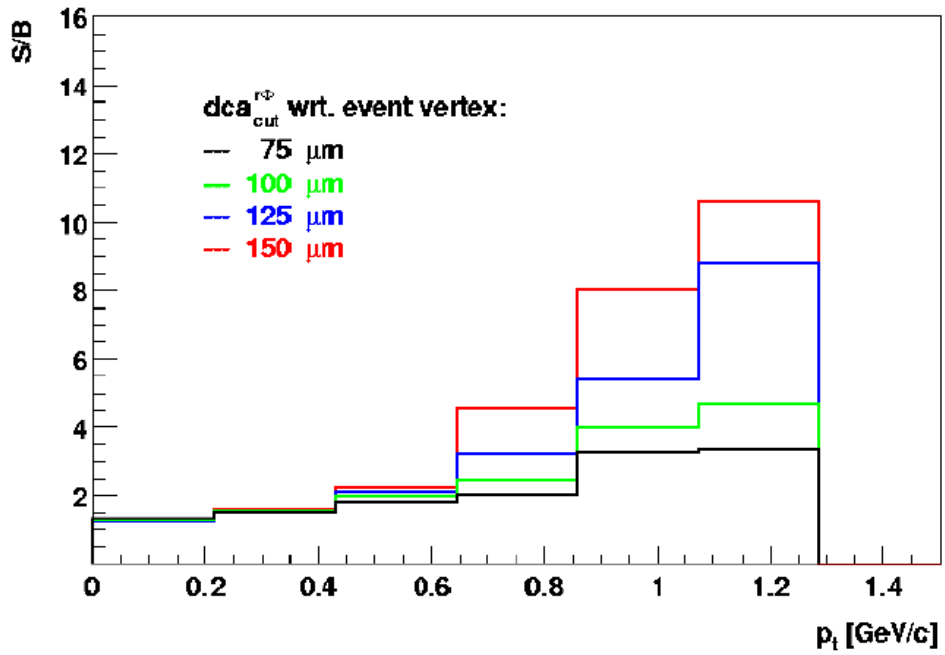

Figure 5: The ratio of charm signal to background electrons from a range of other sources for different values of the DCA cut.

Hadronic decays of D-mesons have the advantage that they can be directly used to find the momentum distribution of identified D's, rather than trying to invert the measured lepton-spectrum to produce an inclusive D-meson spectrum. The difficulty with hadronic decays is that the momenta of the daughter hadrons are low and the large multiple-scattering worsens the displacement resolution of the tracks. To obtain some estimate of how effective the vertex detector might be for measuring hadronic decays we have examined one exit channel, $D^+ \rightarrow K^-\pi^+\pi^+$. This has a branching ratio of 8%. A three-body decay provides very strong constraints, each of the three-tracks must be displaced from the collision point and they must mutually lie within some common feasible decay point. A further constraint is that the mother particle must point back to the collision point. After applying these three constraints to a central Au+Au HIJING events run through the strawman detector produces the three-body invariant mass plot shown in Figure 6.

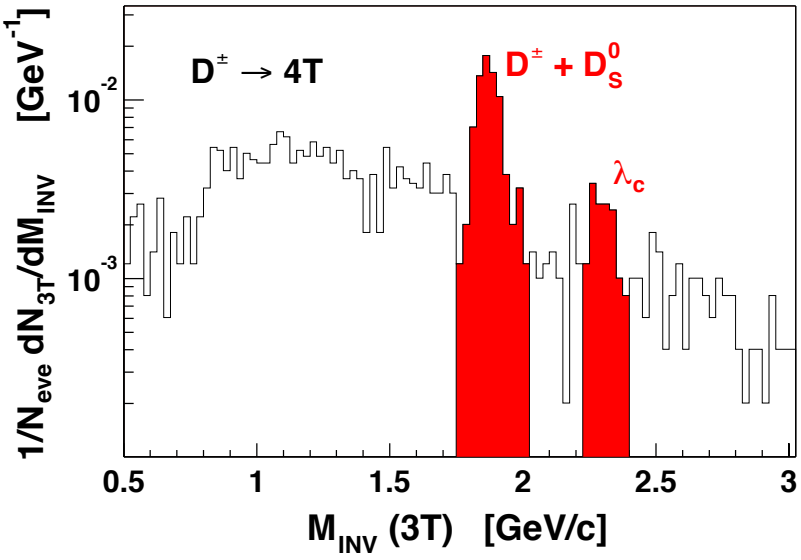

Figure 6: The invariant mass distribution for D candidates for the decay $D^+ \rightarrow K^-\pi^+\pi^+$.

Reconstructed D-mesons and charmed baryons are significantly above the combinatoric background. We have not yet done rate calculations for these decays.

Muon Arms - $D \rightarrow \mu + X, DD \rightarrow \mu^{+-} + e^{-+} + X, DD \rightarrow \mu^+ + \mu^- + X$

Each silicon endcap detector has four layers of pixel detectors which measure the trajectory of particles within the nominal rapidity acceptance of the muon arms. The impact parameter of each track is determined accurately along the Z (beam) direction. For each detected muon, the impact parameter is used to eliminate muons that come from pion and kaon decays. These long-lived decays are the primary source of background muons.

Contrasted with these background muons are "prompt" single muons, which come from more short-lived decays, e.g. open charm and beauty. For transverse momenta below $\sim 5\ GeV/c$ the prompt muons are primarily from semi-leptonic charm decay. Other processes which produce prompt muons, such as J/ψ or

Drell-Yan decays to muon pairs, have much smaller cross-sections times branching ratios. Muons from B decays become important only at larger transverse momenta.

The strategy of our first simulations is to use pp reactions to establish the performance of the strawman detector in measuring open charm and beauty, then to explore how this performance changes within the environment of a heavy-ion collision.

The PYTHIA event generator was used to simulate 5000 semi-leptonic charm decays to muons. The total charm pair cross-section was set at 350 microbarns, which is consistent with recent NLO theoretical calculations and with the published PHENIX measurement at a somewhat lower energy. The decay muons were tracked through the strawman silicon vertex detector and then through the muon spectrometer using PISA.

The mean decay vertex of the detected muons is 785 μm from the interaction vertex. This is ~ 2.5 times larger than the proper decay length of semi-leptonic charm decays (318 μm), due to the lorentz boost. The impact parameter resolution for these muons ranges from 92 to 115 μm, depending on how many total layers of silicon are transversed.

A rate calculation has been performed as follows. Assuming a 350 microbarn cross-section, average p-p luminosity of $8X10^{31}$, 48 days of beam, acceptance time branching ratio of $5.6X10^{-5}$ and two muon arms, about $1.4X10^{7}$ semileptonic charm decays would be recorded. This rate of $\sim 300,000$ per day is before application of a vertex or impact parameter cut.

Production rates for pion and kaons were based upon an parameterization from Hans Boggild which fits the UA1 measurements. The rates were scaled to $\sqrt{s}$=200 AGeV. The resulting pion and kaons are decayed to muons using PYTHIA and then required to satisfy the nominal acceptance of the muon arms.

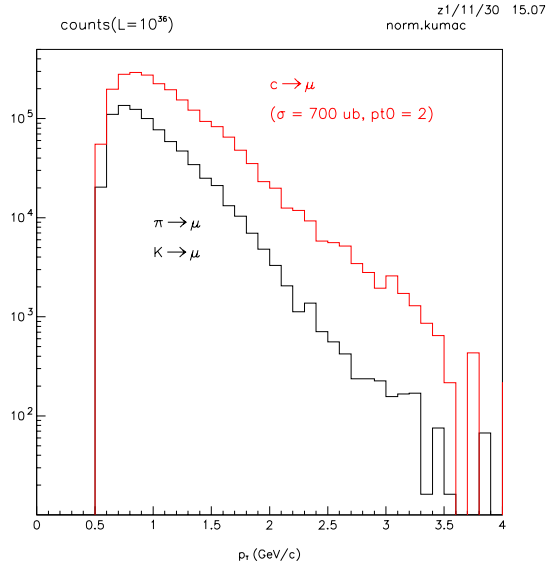

Figure 7: Relative yields of vertex identified muons from charm decays versus pion and kaon decays as a function of transverse momentum.

Figure 7 shows the yield of muons that survive the a loose vertex cut between 1mm and 1cm for both charm decays as well as muons from pion and kaon decays. Note that signal to noise ratio is greater than 2 for $p_T \geq 0.8$ GeV and increases with p_T. Without a vertex detector and the vertex cut, the S/N ratio would be well below 1 for p_T up to ~ 5 GeV. Note that the removal of the muon background from pion and kaon decays could be achieved with a detector with less spatial resolution. The resolution requirement is driven by the physics program of measuring open beauty (see next section).

Since charm is produced in pairs, coincidence measurements of opposite-sign lepton pairs may serve to further enhance the signal to noise in pp and pA reactions. Lepton pairs from charm decay are expected to be a significant background to the low-mass Drell-Yan background. One could use vertex identified muon-electron coincidences to obtain a clean charm pair signal in the rapidity interval midway between the PHENIX central and muon arms.

Tagged Charm Decays - $DD \rightarrow \mu + X, K + \pi$

The signal to noise for exclusive charm decays, such as $D \rightarrow K + \pi$, could be low in heavy ion collisions where the total numbers of kaons and pions produced

is very large. This would lead to a large combinatorial background that could mask the D peak, even with good vertex resolution. By requiring a coincidence of the $D \rightarrow K + \pi$ signal with a prompt muon in the silicon endcap, a significant suppression of the background should be possible. This takes advantage of the fact that charm quarks are produced in pairs and have a large semi-leptonic branching ratio. An open issue is the combinatorics arising from multiple pairs of charm produced in heavy-ion reactions. This channel has not yet been simulated.

5.1.2 Open Beauty Measurements

B meson production, while much rarer than D production, is somewhat simpler to measure. The only real issue is the relatively low rate. There seem to be at least two possibilities;

1. since beauty mesons have a larger lifetime than for charm mesons, it may be possible to extract the beauty yield from the distribution of decay distances. Since the transverse momentum of the leptons is much larger from beauty, a large cut on the p_T of the lepton should help this.

2. the measurement of J/ψ that are displaced from the collision can be used to extract the B-yield (decay channel $B \rightarrow J/\psi$)

Central Arms - $B \rightarrow e + X$**,** $B \rightarrow J/\psi \rightarrow e^+e^-$

These channels have not been simulated for the central arms.

Muon Arms - $B \rightarrow \mu + X$**,** $B \rightarrow J/\psi \rightarrow \mu^+\mu^-$

Beauty decays are accessible through the semi-leptonic decay channel to muons. Since the muon arms have a relatively large acceptance compared with the central arms, counting rates are much less of problem.

The possibility of detecting the decay $B \rightarrow J/\psi \rightarrow \mu^+\mu^-$ appears very promising. Applying a vertex cut on each reconstructed J/ψ has been used successfully to identify B-production in experiments at lower energies. Since the B cross-section is larger at RHIC energies, the measurement should be easier. As the average p_T of J/ψ from beauty decays is much larger than for prompt J/ψ, a p_T cut could also be used to enrich the beauty sample.

Pythia was used to simulate $B \to J/\psi \to \mu^+\mu^-$ decays. The resulting muons are tracked through the silicon and muon spectrometers using PISA. They have an impact resolution of $\sim 55\ \mu$m, significantly better than muons from D decays, due to their larger average momentum. The pair vertex resolution is $\sim 133\ \mu$m, while the mean decay length is ~ 1.1 mm. With a downstream pair vertex cut of 1 mm, 39% of the B decays are retained, while the prompt J/ψ are attenuated by a factor of $2X10^{-4}$. Figure 8 shows the reconstructed Z-vertex distribution for the J/ψ from B decays. Also shown is the vertex resolution. A p_T cut could also increase the signal/background since the mean p_T of the J/ψ from B decay is 2.1 GeV/c, versus about 1 GeV/c for prompt J/ψ.

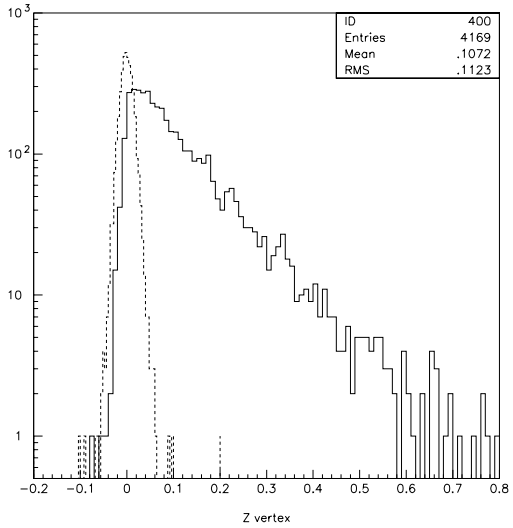

Figure 8: The reconstructed Z-vertex distribution for the J/ψ from B decays (solid line) and the vertex resolution (dashed line).

Using PYTHIA, we estimate that the ratio of $B \to J/\psi$ versus prompt J/ψ is $\sim 0.8\%$, before acceptance corrections. The higher average p_T of the J/ψ from B decays will result in a somewhat lower acceptance than for prompt J/ψ. We have assumed a B cross-section of 2 microbarns and 3 microbarns for the J/ψ. The branching ratio of 1.2% for $B \to J/\psi$ has been previously measured. The total acceptance for these events using both muon arms is $\sim 11\%$. The rate is calculated by assuming a 2 microbarn cross-section, average p-p luminosity of $8X10^{31}$, 48

days of beam, acceptance time branching ratio of $7.8X10^{-5}$ and two muon arms. With these assumptions, about 50,000 beauty decays would be recorded. This rate of $\sim 1{,}000$ per day is before application of a vertex cut. With a realistic vertex cut of 1 mm, 400 events per day could be reconstructed. Even with a factor of 10 lower average luminosity, an excellent beauty measurement is possible.

Exclusive Beauty Decays - $B^{\pm} \rightarrow J/\psi + K^{\pm}$

A measurement of this exclusive beauty decay may be possible in PHENIX. One would use the endcap silicon detector to measure the displaced vertex of the J/ψ and the central arms to identify the kaon. The main issue would be the low rate due to the limited kaon acceptance and the small branching ratio of $\sim 0.25\%$.

5.2 Au - Au Background Issues

Any silicon vertex upgrade must function well with all species of ions, from $p-p$ collisions to central $Au-Au$. The strawman detector has sufficient segmentation to provide low occupancies ($\leq 10\%$ for strips and $\leq 1\%$ for pixels) for all beams. In addition, it must be possible to accurately match tracks in the vertex detector to those recorded in the various PHENIX arms. This is especially important for the muon system, where a significant amount of multiple scattering exists between the vertex detector and the muon tracker. These issues are discussed further in the following sections.

Central Arms - Track Matching to the Vertex Detector.

Tracks from the central arms will be projected back to the vertex detector and matched with hits in each Si layer. This matching has not yet been studied.

Muon Arms - Track Matching to the Vertex Detector.

Occupancies in the silicon endcap detector for central $Au-Au$ collisions can be estimated as follows. We assume a flux of 622 charged particles per unit rapidity with 1.2 units of rapidity coverage. If, for example, the first silicon plane has $\sim 500{,}000$ pixels, then the occupancy is a very low 0.15%. Thus, track finding in the silicon layers should not be difficult.

Tracks in the silicon endcap are bent by the magnetic field of the central PHENIX magnet. The sign of the bend angle provides for charge identification of the particles. From PISA simulations, a four sigma separation between

Table 2: Muon Matching Efficiency

momentum	matching efficiency
3 GeV/c	94%
4 GeV/c	97%
5 GeV/c	100%

positive and negative charges is obtained. Momenta are measured roughly, with $\Delta P/P \simeq 50\%$. By energizing the second set of coils on the central magnet, it is possible to double the magnet field and obtain $\Delta P/P \simeq 25\%$.

PISA simulations show that for muons with momenta corresponding to J/ψ decays, the track match between the silicon endcap and the first muon arm tracking station has a 2 cm sigma in X and Y. For study purposes, a sample of 100 energetic muons were mixed event by event with 100 hijing events. Charged particles with a good track (= 4 hits) in the vertex detector were projected to the first muon tracking station after the magnet steel.The X and Y projections and momentum were compared with those of the simulated track.

The muon matching efficiency, defined as the fraction of events in which the muon track in the vertex detector matched only the same muon's track in the muon spectrometer, was computed. A cut of ± 3 cm in the X and Y match was used, together with a cut of 50% on the signed momentum match (after energy loss correction). The results, given in Table 2, show that the probability of correctly joining the tracks in the vertex detector with those in the muon spectrometer is very high for all momenta.

One potential problem is the possible large background that PHENIX observed when the MUID was first installed. At r=2cm, z=25cm the beam pipe pseudorapidity is the same as the beampipe pseudorapidity in the square hole. There are a considerable number of particles there (outside of the Si acceptance acceptance) that can interact and cause difficulties. What has not yet been done and what will be a high priority in the next simulations is to simulate full HIJING events with a realistic beam pipe.

6 Technology Options

6.1 Hybrid Pixel Detectors

Hybrid active pixel detectors have been developed at CERN and FERMILAB since the late 1980s, for their application in experiments at the Large Hadron Collider (LHC) [24]. Along this path, a series of pixel readout chips of increasing complexity and performance was designed. Several intermediate applications in heavy ion and high energy physics experiments were realized. Experience with pixel detector systems was gained in tracking stations in the fixed target experiments WA97 and NA57. The first application of hybrid pixel detectors in a collider experiment, pioneered by the DELPHI collaboration at LEP for its Very Forward Tracker, operated from 1995 until the end of LEP in 2000.

PHENIX is evaluating two main pixel options, the FPIX series of readout chips developed by FERMILAB[25] and the readout chip of the CERN EP microelectronics group, ALICE1LHCb. The FPIX2 chip will be used at the BTEV experiment at FERMILAB, and the ATLAS experiment at CERN. The ALICE1LHCb chip will be used in the Inner Tracking System of the ALICE experiment [26] and the photon detector of the RICH detector of the LHCb experiment. It is also the building block of the silicon pixel telescope of the NA60 experiment at the SPS that is presently being constructed and is scheduled for its first physics runs in summer and fall of 2002. With an agreement between the ALICE and NA60 Collaborations, readout chips and sensors are provided to NA60 in a common production effort[27, 28, 29]. The PHENIX Collaboration participates in the NA60/ALICE pixel detector project via an engagement of the RIKEN Institute of Physical and Chemical Research, Japan, with the goal to work towards an application of hybrid pixel detectors in a PHENIX vertex spectrometer upgrade.

Because PHENIX colleagues have an an active involvement in testing the ALICE1LHCb chip but not the FPIX chip, more details will be provided on ALICE1LHCb chip. The final decision between these two chips will be based on technical merit, and the experience gained on the NA60 project can be applied to the PHENIX upgrade independent of which chip is used.

6.1.1 The Pixel Front-End Electronics

The ALICE1LHCb pixel readout chip is currently being fabricated in a commercial 0.25 μm CMOS process. Its analog and digital circuitry operates with a 1.6 V power supply. The total static power consumption per chip is about 500 mW.

This active area of the chip of 13.60 mm $\times$ 12.80 mm is divided into 8192 pixel cells of 50 μm $\times$ 425 μm area that are arranged in 32 columns by 256 rows. Every pixel cell itself is divided into an analog and a digital part. The schematics of the components are shown in Fig. 9 [30]. The analog front-end consists of a pre-amplifier followed by a shaper stage with a peaking time of 25 ns. A mask flip-flop allows the pixel to be disabled. A discriminator compares the output of the shaper with a threshold provided globally across the chip. Each pixel contains three logic bits that can be be used to finely adjust the thresholds individually for every pixel to provide pixel-to-pixel threshold uniformity over a full detector system. The outputs of the discriminators in the pixel matrix provide a fast-OR and a fast-multiplicity signal which is output off-chip. In every pixel, the discriminator output is fed into the digital part of the cell. The first stage consists of two digital delay units that store a hit for the duration of the trigger latency. Each delay unit consists of an 8-bit latch which, on receipt of a hit from the discriminator, latches the bit-pattern present onto an 8-bit bus. This pattern is the Gray-encoded contents of an up-down counter whose state changes synchronously with the clock and has an adjustable modulo n. The result of the trigger coincidence is loaded into the next-available cell of a 4-event FIFO, which acts as the multi-event buffer and de-randomizer. This FIFO is read/write addressable by means of two 4-bit busses which carry Gray-encoded patterns. The contents of the FIFO cells waiting to be read out are loaded into a flip-flop by the Level-2 trigger in ALICE and a corresponding signal in LHCb. The flip-flops of each column form a shift register, and the data is shifted out using the system clock. Five latches inside each cell switch on or off the test input to the front-end, mask or activate a pixel and provide three bits of threshold adjustment. The latches have been designed to be resistant to single-event upset.

Using the two delay units, each cell has the capability of simultaneously storing two hits for the trigger latency. The 32 columns are read out in parallel. Using a 10 MHz clock, a complete event is read out from the chip in 25.6 μs. The peripheral logic of the chip contains the counters to address the delay units and the FIFOs. The configuration of the logic and the matrix of pixel cells is performed by means of a serial interface following the IEEE JTAG standard.

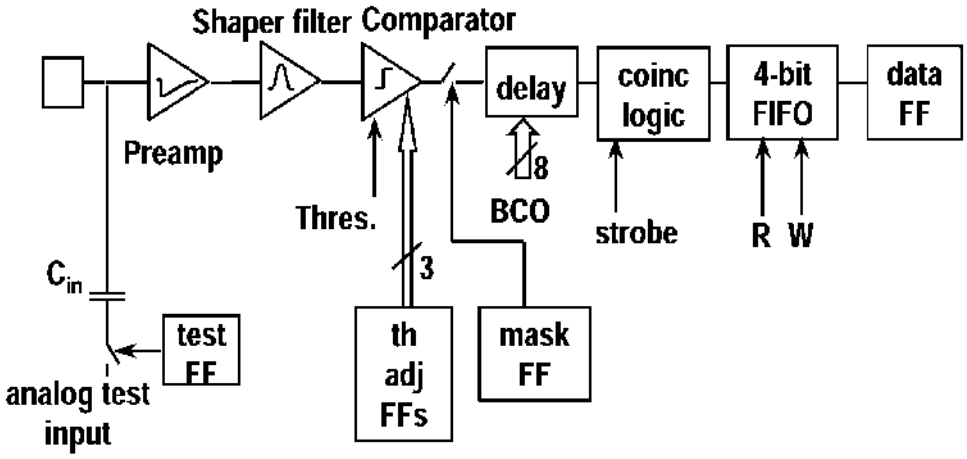

Figure 9: Schematic block diagram of the electronics content of one pixel of the ALICE1LHCb chip.

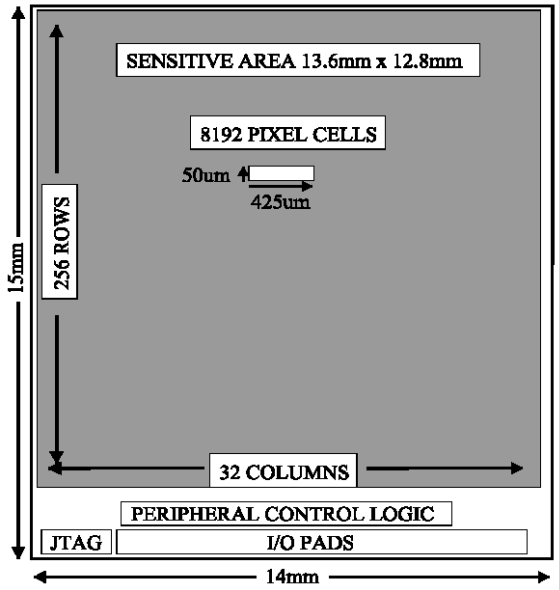

Figure 10: Schematic diagram of the architecture of the ALICE1LHCb chip.

6.1.2 The Pixel Chip Assembly

A pixel chip assembly is an ALICE1LHCb pixel readout chip bump-bonded to a pixel sensor chip. Their relative alignment is assured by the requirement that the 20 μm bonding pad of each readout pixel matches that of the corresponding sensor pixel, for a solder bump to form between them. The sensitive area is a 32×256 matrix of 50 μm $\times$ 425 μm pixels in the sensor chip, matching the dimensions of the pixel readout chip. This active matrix of 13.60 mm $\times$ 12.80 mm is surrounded by a guard ring and a scribe line, adding 560 μm on all four sides. In practice, this may slightly vary, depending on the precision of the dicing and the width of the cut. The sensor chip's thickness is 300 μm for the small planes (wafers ordered in 2001 and present at CERN) and 200 μm for the large planes (joint order together with the ALICE experiment in 2002). Its dimensions may slightly vary due to the dicing precision, too. The chips available to NA60 are presently 750 μm thick. The availability in 2002 of chips from wafers thinned to 300 μm for the plane(s) closest to the target has been negotiated with the ALICE collaboration.

6.1.3 NA60 Detector Cooling

The cooling of the pixel detector planes is intended to be achieved with pipes circulating chilled water on the back side of the hybrid. A study of such a system has been performed [31], with the goal of removing about 1 W of power dissipated per chip and of keeping the sensors at T $\leq$ 20 °C operating temperature. It has turned out that the modest thermal conductivity of Al_2O_3 and the cooling temperatures that are safely applicable in the experimental hall, require the routing of a one-loop copper pipe that is in good thermal contact with an aluminum cooling plate close to the perimeter of the area that is covered by the chips. This structure has recently been attached to the ceramic with silicon (i.e. non-rigid) glue to compensate for the different thermal expansion coefficients of the components. The first assembled pixel detector plane is presently being used to actually measure the effectiveness of the cooling system in the laboratory, while trying to minimize the extra material involved. First measurements indicate that operating temperatures of the chips of approximately 25 C can indeed be achieved at the present time, while without cooling the temperatures exceed 70 C.

6.1.4 Timeline of NA60/ALICE and Possible Availability of Components to PHENIX

The successful test of the first 4-chip prototype plane validated the design and construction of the hybrid and the PCB for the NA60 Silicon Pixel Telescope. The NA60 specific readout electronics and software is well advanced and will be used soon for testing the individual pixel planes. The NA60 collaboration aims at the full pixel detector telescope installed in the experiment for the heavy ion run in fall 2002. The challenge of the production, assembly and integration of the full number of detector planes may not be met before Oct 2002 due to the extremely short time, dependence on timely industrial supply, and only a small team of experts involved. The production and assembly will continue for the physics runs in the year 2003.

This means that the details on the readout system, and a test stand with all relevant components including a reference chip card or even an operational detector module, could be made available to PHENIX towards the end of the year 2002. This would allow the PHENIX collaboration to perform detailed studies on an interface of the CERN pixel electronics to the PHENIX readout system. Table 3 compares some of the important characteristics of the ALICE and NA60 experiments with the matching requirements of PHENIX. A possible scheme of how such an interface is illustrated in Fig. 11.

The detectors and readout chips presently available to ALICE (and NA60) do not yet meet the material budget that can be tolerated. This statement is also valid for a possible application of the CERN pixel technology in a PHENIX vertex spectrometer. The ALICE Collaboration has started negotiations with the chip foundry VTT in Finnland to undertake an effort in the production of thinned assemblies. It is technically feasible to thin readout chips from standard 750 μm thickness down to approximately 150 μm, which can still be handled during the process of bump bonding to sensors of about the same thickness. It is expected that such an effort will yield chips and modules in about one year's time (middle 2003), with a likely thickness of 200 μm for the electronics and $\leq$200μm for the sensors. Study objectives will be the production yield of bump bonded assemblies, handling issues and performance of those devices. Together with ALICE, the construction of a pixel detector module that matches the PHENIX requirements, could be undertaken from around that time.

The integration of one or two pixel detector barrels in a silicon vertex detector of PHENIX, together with micro-strip detector layers on the same mechanical support, could be envisaged for the year 2005.

	ALICE	NA60	PHENIX
occupancy	average 1%	max. 10%	approx. 1%
trigger latency	5.5 μs	1.3 μs	$<$4.3 μs
average trigger rate	a few kHz	1.6 kHz	10kHz
full event readout	400 μs	400 μs	40(80) μs
readout clock	10 MHz	10 MHz	$>$10 MHz
charge signal	12 000 e	12 000 e	$\leq$12 000 e
pixel cell size	50×425 μm^2	50×425 μm^2	50×425 μm^2
max. power/channel	100 μW	100 μW	100 μW
total detector area	1.2 m^2	0.02 m^2	approx. 0.5 m^2
radiation dose	$<$500 krad/10y	1 Mrad/week	known?

Table 3: Comparison of specifications of pixel detectors in heavy ion experiments at CERN with PHENIX requirements.

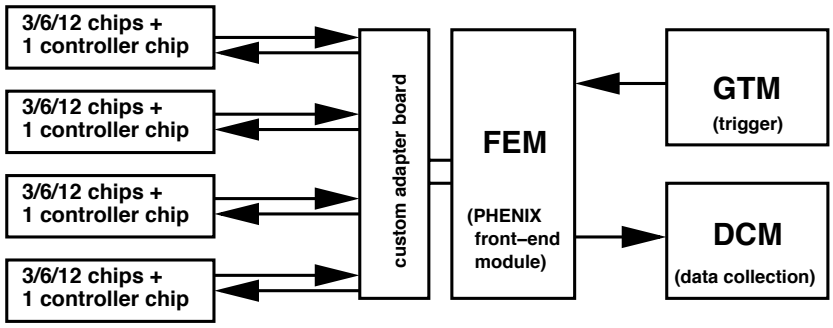

Figure 11: Schematics of a possible interface of a ALICE/NA60 pixel detector module to the PHENIX readout system.

6.2 Monolithic Pixel

Monolithic pixel detectors incorporate the sensor and read-out electronics in one Si chip. Ionization electrons from the epitaxial or substrate layers diffuse to a collection well and are processed with on-pixel electronics similar to that in the

hybrid pixel. The potential advantages include a reduction in complexity, thickness and possibly cost.

This technology is not yet ready for full use in an high-energy experiment. However in recent years progress has been driven by commercial applications rather than physics applications. Active Pixel Sensors (APS) are monolithic devices, where electrons from the photo-electric effect are produced in the Si substrate and processed by on-pixel electronics. APS devices have been developed for digital cameras[32] where they are in commercial production.

In physics, groups at LEPSI/Strasbourg[33] and Hawaii[34], have been adopting APS technology to physics use. The Strasbourg group has developed a series of MIMOSA chips[33] to demonstrate that sufficient ionization electrons can be collected to produce signals well above the noise level. The MIMOSA chip required a custom CMOS process to produce an epitaxial layer of 17μm since the conventional process produces an epitaxial layer of a few microns at most. Even with such a thick, custom epitaxial layer the number of ionization electrons is a factor of ten smaller than for a hybrid-pixel detector where the sensor thickness is on the order of a few hundred microns. Since the signal is smaller, electronic noise is a critical issue.

The LEPSI group has not concentrated on a fast-readout since their planned application is at electron colliders where the event rate is lower. In their design, the signal on each pixel is held by a sample and hold, until amplified/digitized by one circuit for the whole device. To speed this up without sacrificing noise performance, the Iowa State group has adapted the MIMOSA design by placing an amplifier and ADC at the base and top of each column[35].

Correlated noise on the pixels has been a problem for the MIMOSA designs[36]. To reduce this, the Iowa State group has designed a read and read-again system for each pixel to subtract the correlated noise during amplification. The first version of this design will be submitted to MOSIS in June 2002[35].

6.3 Si Strips

The outer three barrel layers of the silicon detector will be instrumented by silicon strips. Silicon strip detectors themselves are a well-established technology, and several suppliers are available worldwide. The matching readout electronics is another matter. It is planned to implement the Si strips on a short timescale so a suitable choice needs to be made from existing designs that match the PHENIX readout criteria.

For the detectors themselves, the group is considering two choices; the first is standard, well-established Si strip detectors that are commercially available, e.g. from Hammamatsu, or to use a new form of the detectors developed and fabricated by BNL instrumentation[37]. The plan is to test these two options in the Fall 2002.

The BNL detectors are 80μm pitch, 3x6cm single-sided sensors. Two sets of read-out strips are placed longitudinally and diagonally, providing simultaneous x-u readout from a single surface. At low-occupancies this projective geometry localizes a hit to with a pad of $80x800\mu m$. Each strip detector has $\sim$ 1500 channels (375 channels per end, 2-readouts per end and two ends per detector). Depending on final layout plan, the total number of channels is 200 to 300K, so we will need on the order of 2000 readout chips

6.4 Si Strips Readout Electronics

We plan to make a choice from among the currently available electronics. There are several candidates:

6.4.1 NA60 strip electronics

SCTA128-VG chip: This is a 128-channel chip, with pipelines and buffers, which can accomodate an input capacitance of 15 - 20 pF, and puts out a digitized data packet. Full details are in the references[38]. The chip measures 8x8mm, and has $60\mu m$ pitch input traces and is fabricated using the rad-hard DMILL process, which seems to have low-yield, 20%, and is likely to be phased out during 2003. ATLAS will have completed their production by then, so they are not considering changing. One issue will be whether we could get a production run of these chips.

The chip matches the PHENIX requirements:

1. amplifier peaking time ($25ns$) smaller than RHIC beam crossing timing ($106ns$)
2. L1 trigger latency ($4.3\mu s$) matches depth of analog pipeline ($128x25ns = 13.6\mu s$)
3. 8 bit de-randomizing buffer: max. speed to fill it up: 8 consecutive positive triggers $\rightarrow 8x106ns = 832ns = 0.8\mu s$ but in reality if fills up slower; buffer cannot be overwritten, if full, it creates dead time
4. 40 MHz sampling: readout of one buffer column in $3.2\mu s$

(a) this compares to $40(80)\mu s$ readout time per subsystem per event.

(b) several chips can be chained for readout, module construction is possible

(NA60 hybrid: 6 chips, of which pairs of 2 are read out together)

It seems that this chip can be successfully operated in the PHENIX environment.

6.4.2 Atlas ABCD chip

The Atlas ABCD chip[39] shares ancestry with the SCTA128-VG chip and therefore has many of the same features. It is a 128-channel chip, housed on 6.6x8.4 mm, fabricated in a rad-hard DMILL process, with the same concern about yield and availability. The input pitch is 50 microns. The preamp has 25 ns peaking time, followed by a discriminator that has a level common to all 128 channels, plus 4 trim bits to fine-tune the discriminator levels. The digital signal flows into 132-cell pipeline. Upon triggering, events are transferred to an 8-event-deep derandomizing buffer, and compressed data packets are read out using a token-ring scheme that allows the readout of up to 6 chips on one optical fiber channel. Power consumption is less than 2.5 mW/channel.

6.4.3 SVX4

The SVX family of chips has been developed at at Fermilab[40]. The SVX4 uses 0.25um CMOS technology which is broadly available. It is an 128 channel chip with a 46 deep pipeline cycled by the beam-crossing clock. The rise time is on the order of 60ns and the output of the chip is an ADC word (how many bits?) per channel. Currently the amplifier and ADC have been separately tested, and as of April 2002 the full chip has been submitted to MOSIS but not yet tested.

6.4.4 APV25

The APV25-S1 is a 128 channel analogue pipeline with 192 columns of analogue storage[41]. The signals are amplified into 50ns shaped pulses of magnitude 100mV / 25,000 electrons. These are sampled at a rate of 40MHz and stored in the pipeline. Useful data are marked after a programmable latency, and held in the pipeline until such a time that they can be read out. A 32 deep FIFO holds the addresses of pipeline columns holding marked data. Other data (which is not considered useful) is overwritten. When data is read from the pipeline it is processed

using a filter before being read out through an analogue multiplexer and driven off chip as a differential current. The digitization is done off the detector.

6.4.5 MVD electronics

The current MVD silicon detector has strip detectors with $200\mu m$ pitch. The front-end electronics use the Oak Ridge 32-channel TGV preamp/analog pipeline storage chip[42] and the generic PHENIX ADC chip. The TGV-32 has an integrating preamp, followed by a 64-deep analog pipeline with simultaneous read/write capability, where integrated charge is written every beam crossing. Upon receiving a trigger, a pre-post analog subtraction is performed on the contents of the relevant AMU cells, followed by digitization in the ADC chip, and formation of a data packet by an FPGA.

Data packets are sent to nearby electronics where they are converted to standard PHENIX data packets on optical fiber. Obviously, a complete chain of electronics that matches the PHENIX environment is available. One concern is that this chain of electronics has not yet worked reliably.

For the MVD, the TGV-32 and ADC chips are packaged onto 256-channel MCM modules that have $200\mu m$ input pitch, to match the strip detectors. The bare TGV chips themselves have a much finer input pitch, and could be packaged to match the smaller pitch of the new detectors.

6.5 VA2 chip

The VA2 chip is a descendant of the Viking 128-channel CMOS chip, developed at CERN in the early 90's. The VA2 chip [10] is a 128-channel chip made to match $50-\mu m-pitch$ strip detectors, with 5-20 pF strip capacitance. The preamp has a $1-3\mu s$ peaking time, and a nominal gain of 30mV/pC. It is followed by a shaper, and a sample-and-hold. Data bits are shifted out from a 128-cell bit register.

The $1\mu s$ peaking time is much longer that what is needed in the PHENIX environment, and therefore this chip cannot be used for the new silicon detector.

7 Mechanical requirements, stability, cooling

The mechanical requirements for a silicon vertex detector are derived from the spatial resolution needed, heat load of the electronics, radiation length restrictions, utility routing, maintainability, and the local radiation environment. Satisfying all

of these non-trivial objectives at times requires the use of special materials and designs.

7.1 Mechanical Structures

On the basis of simulations the stability requirement for the silicon tracker is 25 microns. In addition, the radiation length budget for the mechanical structures including utilities must be less than 0.5% so that multiple scattering does not adversely affect the spatial resolution. As a baseline the detector is expected to operate at room temperature and experience a temperature fluctuation of 5 deg F. These requirements dictate that the structural material must,

1. have a high stiffness-to-weight ratio which implies a high modulus and a low Z material
2. short and long term stability
3. low coefficient of thermal expansion (CTE)
4. good thermal conductivity
5. modest cost and machinable

Materials that can be considered to satisfy these criteria are beryllium, carbon fiber composites, metal matrix composites, and carbon-carbon composites. Past and present vertex detectors have used all of these. The SLD vertex detector used beryllium as the structural material primarily because the detector operated in a cooled environment. The ATLAS detector has selected carbon-carbon and ALICE has chosen a high-modulus carbon fiber composite for the support material for their respective vertex detectors. The specific choice for the PHENIX silicon vertex detector will depend on it's specific geometry and environment but will most likely not be beryllium.

The four layers of barrel is nominally a layer of pixel detectors close to the beam pipe and three layers of strip detectors at outer radii. The azimuthal coverage will be +-(22.5-112.5)deg and eta = +-0.35. The forward region will have up to 4 disks of pixel detectors and will have full azimuthal coverage and eta coverage for the north(south) regions = 1.15(1.24)-2.44.

For the barrel region the ALICE ITS (Inner Tracking System) is a good model for what will be needed. Ladders composed of rectangular pixel detectors and electronics will form the logical unit. For the forward regions a possible model may be from the BTev collaboration.

7.2 Cooling

To estimate the cooling requirements we have used the ALICE ITS (Inner Tracking System) design parameters. For the pixel detectors it expected that the heat load will be 0.7 watts/cm**2 uniformly distributed across the detectors. For the strip detectors the heat load of 0.5 Watts will be concentrated at the ends of the strip detectors. Thus, we expect different cooling requirements between the pixel detectors and the strip detectors and this will impact the mechanical design. The ALICE detector uses water for cooling and this will most likely be the approach that we will pursue.

7.3 Utilities

Providing power and cooling and still maintaining the radiation length budget is probably one of the more challenging aspects of the mechanical design. The mechanical structure must be able to support the silicon detector ladders as well as the weight of the utilities. In the barrel region providing the power and signal lines and cooling manifolds without adversely affecting the forward regions yet maintaining good acceptance will be very difficult. Low mass cables such as aluminum-Upilex microcables will be used for both power and signals. Routing will be in areas that are not in the acceptance where ever possible.

7.4 Environmental conditions

An environmental enclosure will be part of the design so we can control environmental conditions such as humidity, RF noise, dust. etc.

7.5 Global requirements

The silicon vertex detector is positioned around the beryllium beam pipe and between the central magnet pole pieces. The detector will be in two half cylinders so that it can be installed and removed without the necessity of removing the beam pipe. The detector will be kinematically mounted off of the magnet pole pieces to reduce stresses that may occur from the central magnet.

8 Next Steps

The zeroth-level performance of strawman detector of four barrel layers and endcaps with four disks has been simulated. Open charm and yields and spectra can be measured over a broad range of rapidity via three decay channels: electron decay, muon decay and hadronic decay. Open beauty also seems feasible via displaced J/ψ vertexes. These measurements will provide new physics opportunities for the spin, pA and AA programs.

It is time to move from the strawman detector to a more realistic layout with the candidate technologies, i.e. commercial Si-strip with e.g. SVX4 readout and ALICE pixels. Though not bound to such a choice, it is important to perform more detailed simulations to confirm that the physics goals can be met with a realistic layout. One large open issue is the radial extent and pixel size for the endcap disks. This is being actively worked on.

Some of the technical issues have been identified and R&D is being carried out

1. a telescope of BNL-Si-strip sensors is being bench-tested in summer/early Fall 2002

2. readout electronics for Si-strips are being evaluated

3. a team is in place at CERN working with the ALICE pixel team, implementing a pixel detector for NA60.

4. the first MOSIS submission in June 2002 for the monolithic pixel by the ISU group.

5. the details of the pixel layers (size, heat load, mechanical support etc.) are being defined to decide whether it is feasible to design the mechanical structure of the full barrel and endcaps. The alternative is to design a support for the Si strip detector and to replace it when the pixel design is ready.

References

[1] R.L. Jaffe hep-ph/0201068 and references therein

[2] G.T. Bodwin et al., Phys. Rev. D 51, 1125 (1995), E. Braaten, Nucl. Phys A 610 (1996), A. Sansoni, NUcl. Phys. A. 610, 373 (1996).

[3] I. Sarcevic, P. Valerio, Phys. Rev C. 51, 1433 (1995)

[4] M. Krämer hep-ph/0106120, M. Cacciari et al., hep-ph/9803400, M. Stratmann, Eur. Phys. J. C10, 107 (1999)

[5] R. Vogt hep-ph/0111271

[6] E. Norrbin, T. Sjostrand, Eur. Phys. J. C 17, 137 (2000)

[7] M. Arnedo, Phys. Rep. 240, 301 (1994), K.J. Eskola et al., hep-ph/9906484

[8] T. Gousset, H.J. Pirner Phys. Lett. B 375, 349 (1996)

[9] L. Frankfurt and M. Strikman, Eur. Phys. J. A5, 293 (1996)

[10] M. Cacciari hep-ph/9803400

[11] E. Shuryak Phys. Rep 61, 71 (1980)

[12] P. Levai et al, Phys. Rev C. 51, 3326 (1995)

[13] Z. Lin and M. Gyulassy, Phys. Rev. C. 51, 2177 (1995)

[14] D. Kharzeev et al., Z. Phys. C. 74, 307 (1997)

[15] R. Baier, D. Schiff, B.G. Zakharov, Ann. Rev. Nucl. Sci 50, 37 (2000)

[16] U.A. Wiedemann, Nucl. Phys. B 588, 303 (2000)

[17] M. Gyulassy et al., nucl-th/0006010

[18] M. Mustafa et al., Phys. Lett. B 428, 234 (1998)

[19] M. Mustafa et al., Phys. Rev. C 57, 889 (1998)

[20] I.P. Lokhtin, A.M. Singer, Eur. Phys. J. C 17, 137 (2000)

[21] Z. Lin, R. Vogt, X.-N. Wang, Phys Rev C 57, 899 (1998)

[22] Z. Lin, R. Vogt, Nucl. Phys. B 544, 339 (1999)

[23] K. Adcox et al., Phys. Rev. Lett. 88, 19203 (2002)

[24] Heijne, E.H.M., *Semiconductor micropattern pixel detectors: A review of the beginnings*, Nucl. Instrum. Methods Phys. Res. A465 (2001) 1-26

[25] http://fnalpubs.fnal.gov/archive/2002/pub/Pub-02-076-E.html

[26] The ALICE Collaboration, *ALICE - Technical Design Report of the Inner Tracking System*, CERN/LHCC 99-12, 18 June 1999

[27] NA60 Collaboration, *Proposal: Study of Prompt Dimuon and Charm Production with Proton and Heavy Ion Beams at the CERN SPS*, SPSC/P316, 7 March 2000

[28] NA60 Collaboration, *NA60 status report*, CERN/SPSC/M662, 12 March 2001

[29] NA60 Collaboration, *NA60 status report*, CERN/SPSC/M679, 12 March 2002

[30] W. Snoeys et al., *Pixel readout electronics development for the ALICE pixel vertex and LHCb RHICH detector*, Nucl. Instr. Meth. Phys. Res. A465 (2001) 176–189

[31] A. Onnela, *Estimates on the NA60 Pixel Cooling*, internal note CERN EP-TA1 group, 18 December 2001

[32] optical Active Pixel Sensors www.photobit.com where they are in commerical production.

[33] , R. Turchetta et al., Nucl. Inst. Meth. A458, 677 (2001)

[34] C. Kenney et al., Nucl. Inst. Meth. A342, 59 (1994) , Nucl. Inst. Meth. A395, 328 (1997)

[35] T. Tanadi et al., http://p25ext.lanl.gov/ hubert/phenix/silicon/Report.pdf

[36] G. Deptuch, private communication

[37] http://ssd-rd.web.cern.ch/ssd-rd/rd/talks/Li-rd-2001.pdf

[38] SCTA128VG Specification ver. 1.2:
http://chipinfo.web.cern.ch/chipinfo/docs/scta128vg_spec1.pdf
Perfomance of a 128 Channel Analogue Front-End Chip for Read-Out Si Strip Detector Modules for LHC Experiments,
http://chipinfo.web.cern.ch/chipinfo/docs/N6-3_REV.pdf
The NA60 silicon tracking telescope for proton running.

http://na60.web.cern.ch/NA60/notes/note_2001_5.ps.Z

[39] Atlas ABCD chip, http://chipinfo.web.cern.ch/chipinfo/
Design and Performance of the ABCD chip for the binary readout of silicon strip detectors in the ATLAS Semiconductor Tracker, W. Dabrowski et al., IEEE Trans.Nucl.Sc.47, No 6, December 2000.

[40] http://www-cdf.lbl.gov/users/mweber/svx4

[41] http://www.te.rl.ac.uk/med/projects/High_Energy_Physics/CMS/APV25-S1/pdf/Overview.pdf

[42] TGV32: A 32-channel preamplifier chip for the Multiplicity Vertex Detector at PHENIX.
C. L. Britton, et al., Review of Scientific Instruments, Vol. 70, No. 3, pp. 1684-1687, March 1999.
http://p25ext.lanl.gov/phenix/mvd/notes/1998/PHENIX-MVD-98-11/IEEE97paperhtml.html

[43] VA2 chip, produced by IDE in Norway. http://193.216.193.195/download/ASICdocuments/VA2.pdf